Journal of Renewable Materials

Tech Science Press

DOI: 10.32604/jrm.2022.023011

check for updates

ARTICLE

Towards Solar-Driven Formation of Robust and Self-Healable Waterborne Polyurethane Containing Disulfide Bonds via *in-situ* Incorporation of 2D Titanium Carbide MXene

Sai Gong[1,2,#], Shanglin Xiang[1,#], Tingwei Wang[1,*] and Dongyu Cai[2,*]

[1]College of Materials Science & Engineering, Nanjing Tech University, Nanjing, 211816, China

[2]Key Laboratory of Flexible Electronics (KLOFE) & Institute of Advanced Materials (IAM), Jiangsu National Synergetic Innovation Center for Advanced Materials (SICAM), Nanjing Tech University, Nanjing, 211816, China

[*]Corresponding Authors: Tingwei Wang. Email: wangtw@njtech.edu.cn; Dongyu Cai. Email: iamdycai@njtech.edu.cn

[#]These authors make equal contribution to this work

Received: 05 April 2022 Accepted: 13 June 2022

ABSTRACT

Waterborne polymers are vital for coating industry to reduce carbon emissions. However, formation of robust and self-healable films at ambient temperature remains a challenge owing to high energy cost of film formation process. This work reports a solar-driven film formation of waterborne polyurethanes (WPUs) containing disulfide bonds via *in-situ* incorporation of 2D titanium carbide (MXene) with ability to convert light to heat. Instead of directly mixed with WPUs, MXene is added to join the reaction with isocyanate-terminated pre-polymer before emulsification process. This approach not only prevents aggregation of MXene in water but stabilizes MXene against thermal degradation which is the key hurdle for mass production of MXene/WPU composites. More importantly, our results show that mechanical performance of WPU films under visible light (100 mW/cm^2) is overwhelmingly competitive with that processed in oven. Furthermore, the existence of disulfide bonds in PU chains enables fast self-healing of micro-cracks under natural visible light which could vanish completely within 40 min. The fractured specimens were repaired under natural visible light for 2 h, and the self-healing efficiency of tensile strength and elongation at break reached over 94.00%.

KEYWORDS

MXene; waterborne polymer; photothermal conversion; film formation

1 Introduction

The coating industry is the main source of carbon emission since solvents are widely used to tune the flowing ability of polymers [1–3]. In addition, the volatilization of organic solvents causes air pollution. In the past decades, Waterborne polymers (WPs) have attracted huge attention in both academia and industries in virtue of their advantages of eco-friendly nature and low toxicity [4–6]. Solvent-free Waterborne polymers are considered as one of the solutions to reduce the carbon emission from the coating industry and reduce air pollution [7,8]. However, there are two key problems hindering the full replacement of traditional solvent-based polymers (SPs) by WPs. Firstly, a high energy cost is required for the evaporation of water, and this makes the use of WPs outdoors extremely difficult at ambient temperature. Secondly, WPs exist as a form of

latex with polymer particles dispersed in water [9,10]. This is different from SPs with entangled polymer chains in organic solvents. WPs gain strength through a close pack of polymer particles driven by evaporation of water which is generally called film formation. By comparing with SPs, the evaporation rate of water seriously affects the interfacial diffusion and entanglement of particles in WPs. Moreover, the film-forming strength of WPs is affected by the content of carboxyl and amino groups, the proportion of salt-forming groups, and the relative humidity in the air. Therefore, they always demonstrate a poor mechanical performance in comparison with SPs [11,12].

Natural sunlight is able to generate 4.4×10^4 megajoules of green and renewable energy for the earth per hour [13]. MXene is a new 2D nano-layered material produced by selectively etching the a layer from the MAX phase [14–16], which demonstrates an exceptional ability for converting light to heat with the efficiency of nearly 100% due to strong absorption of electromagnetic waves by semi-metalized interlayer structure [14,17]. More interestingly, the combination of metallic basal plane and oxidized surface renders MXene conductive yet hydrophilic. Therefore, it is not a painful process for the incorporation of MXene into WPs for developing functional composite materials. However, the application of MXene in WPs is still challenging as MXene tends to be oxidized in water [18,19]. Recently, our group found that surface graft of MXene with polymer ionomers could stabilize MXene in the water against thermal degradation [20]. On the basis of this work, we further take waterborne polyurethanes (WPUs) as a model system and explore the effect of MXene nanosheets on the film formation of WPUs under 100 mW/cm^2 visible light that is mimic natural sunlight. With effective photothermal conversion on the MXene nanosheets, water is quickly evaporated just under visible light, and more importantly, the mutual accumulation of particles is enhanced for forming robust films owing to the settlement of MXene among the particles. Furthermore, we also demonstrate that the self-healing of micro-cracks is accelerated with the incorporation of disulfide bonds into PU chains. This strategy is not only energy-saving but also makes it possible for processing WPU outdoors.

2 Material and Methods

2.1 Raw Materials

Lithium fluoride (LiF) and titanium aluminum carbide (Ti_3AlC_2) were obtained from Shanghai Aladdin Chemistry Co. Ltd. (China) and Laizhou Kaiene Ceramic Material Co., Ltd., China), respectively. 2-hydroxyethyl disulfide (HEDS) was obtained from Shanghai Aladdin Chemistry CO. Hydrochloric acid (HCl), dibutyltin dilaurate (DBTDL), ethylenediamine (EDA), and triethylamine (TEA) were purchased from Shanghai Lingfeng Chemical Reagent Co., Ltd. (China). Polyether diol (N210, Mn = 1000) and 2, 2-dimethylol propionic acid (DMPA, Aladdin Reagents Co., Ltd., China) were dried at 110°C and 70°C for 4 h in a vacuum oven, respectively. Isophorone diisocyanate (IPDI) was used as received. Acetone was purified by 4 Å molecular sieves.

2.2 Preparation of Delaminated $Ti_3C_2T_x$-MXene Nanosheets

Firstly, 1 g LiF was mixed with 20 mL 9 M HCl for 5 min. Then, 1 g Ti_3AlC_2 powder was slowly added into the LiF/HCl solution, and the mixture was stirred at 35°C for 24 h. Afterward, the mixture was rinsed several times via centrifugation until the pH reached 6. The mixture was top up with deionized water and vortexed for another 24 h. Finally, the solution was centrifuged at 3500 rpm for 60 min. The supernatant (MXene dispersion) was collected for further use.

2.3 Preparation of MXene/WPU (I-SHWPU) Composite by in-situ Polymerization

As shown in Scheme 1: At first, N210 (15 g), IPDI (10 g), and DBTDL (0.08 g) were added into a three-neck flask with a mechanical stirrer, thermometer, and reflux condenser. The reaction was carried out at 85°C for 2 h. Then, DMPA (1.65 g) was added into the flask to carry out the chain extension reaction at 85°C for

1 h. After cooling to 60°C, HEDS (1.12 g) was added into the flask to carry out the chain extension reaction for 6 h. After cooling to 40°C, TEA (1.24 g) was added to neutralize the carboxylic groups from DMPA for 10 min. At this point, an anionic polyurethane was achieved with a terminal of isocyanate (NCO) group. Then, MXene supernatant (MXene content accounts for 0.15% of polyurethane) was added to stirred for 5 min. Afterward, deionized water was added dropwise for emulsification and EDA was added for further chain extension. Finally, acetone was removed by rotary evaporator and the waterborne polyurethane emulsion with a solid content of 30 wt% was obtained.

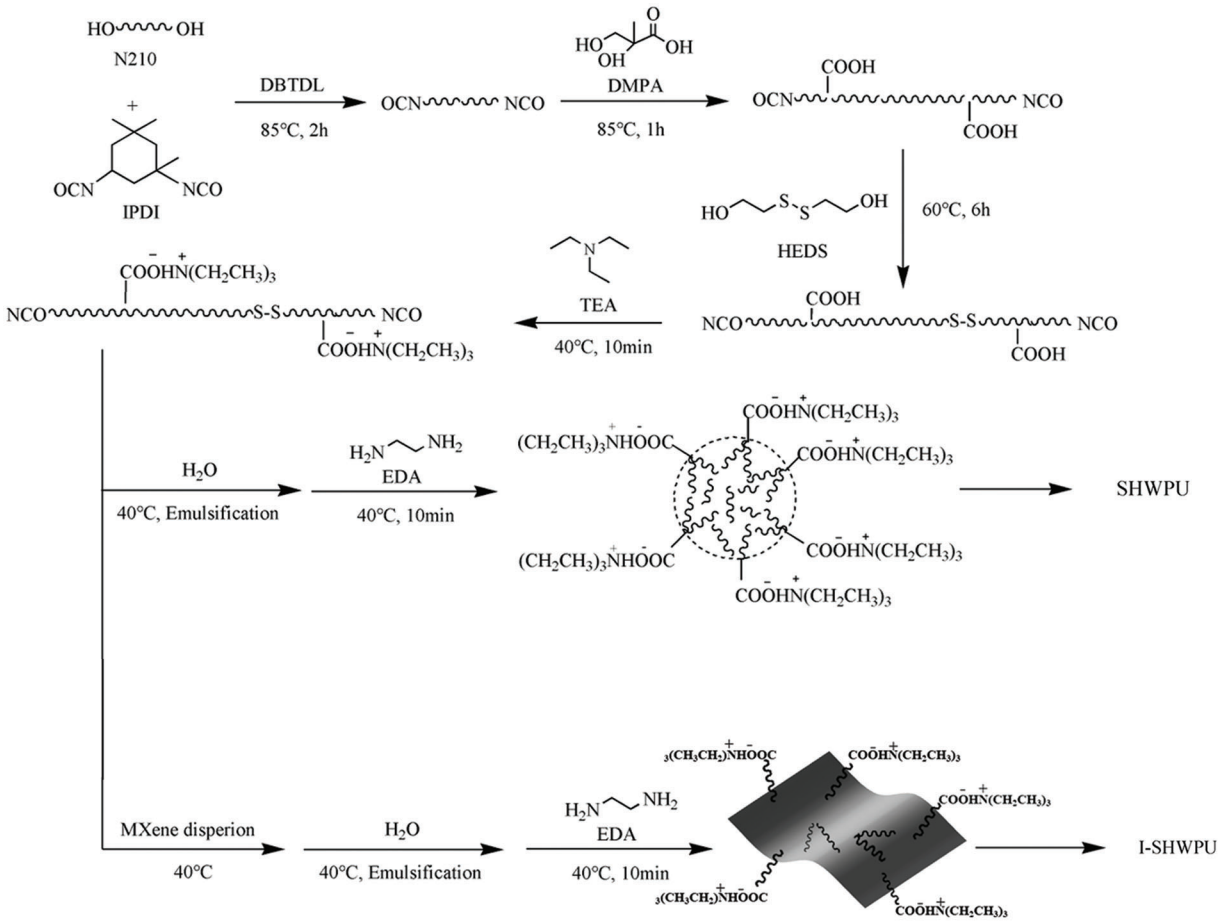

Scheme 1: Synthesis diagram of SHWPU and I-SHWPU emulsions

2.4 Preparation of I-SHWPU and D-I-SHWPU Film

I-SHWPU emulsion was poured into a polypropylene plate (7 cm × 8 cm) and dried at ambient temperature for 3 days. Finally, the films (I-SHWPU) were irradiated under a 100 mW/cm^2 visible light for further drying for 36 h. For comparison, the films were dried in an oven at 55°C for 36 h, which is designated as D-I-SHWPU.

2.5 Characterization

Fourier Transform Infrared (FTIR): I-SHWPU film was tested using Fourier transform infrared spectrometer (Nexus-670). The scan range was from 4000 to 500 cm^{-1} with a resolution of 4 cm^{-1} for a total of 32 times. *In situ* Raman spectroscopy: The Raman spectra were obtained from Labram

HR800 Raman spectrometer under a laser with a wavelength of 514 nm. X-ray Diffraction (XRD): X-ray Diffraction (XRD) measurements were conducted from 3° to 80° at a scan rate of 10° min^{-1} by using a Rigaku X-ray diffractometer. Scanning Electron Microscopy (SEM): The morphology of Ti_3AlC_2, MXene, and the fractured surface of films were observed by scanning electron microscope (SEM; JEM-6510). Particle size analyzer: The OTSUKA analyzer (NanoPlus-3) was used to characterize the Zeta potential and particle size distribution of polyurethane emulsions and MXene dispersion. X-ray photoelectron spectroscopy (XPS) analysis was carried out by a Thermo ESCALAB 250XI spectrometer. The UV-Vis spectra of the films were measured on a Shimadzu UV2600 spectrophotometer. Differential Scanning Calorimetry (DSC): The glass transition temperature (T_g) of the composite film was tested using the American TA thermal analysis Q-20, the test range was −80°C–150°C, and the nitrogen atmosphere was 10 ml/min. Visible light sources: Xenon lamp with a cutoff filter ($\lambda >= 420$ nm), CEL-HXF300, Beijing China Education Au-light Co., Ltd. Optical Microscope: Self-healing of the scratches on films was observed using Leica optical microscope (DM 2500P). Mechanical properties: The composite films were cut into 75 × 4 mm dumbbell-shaped samples. Then, the tensile strength and elongation at break were tested using a universal testing machine (CMT 5254) with a tensile rate of 300 mm/min.

3 Results and Discussion

In-situ incorporation of MXene into WPUs shown in Scheme 1 could be briefly described as follows: polyol (N210) and di-isocyanate (IPDI) react to form a prepolymer with -NCO group at both ends. Afterward, 2, 2-dimethylol propionic acid (DPMA) and 2-hydroxyethyl disulfide (HEDS) act as chain extenders to react with NCO-terminated prepolymer to introduce carboxylic groups onto the side and disulfide bonds into the backbone of polyurethane, respectively. Subsequently, the addition of triethylamine (TEA) neutralizes the carboxylic group to improve the hydrophilicity of polyurethane chains. Prior to adding deionized water for emulsification, MXene is added to react with the residual-NCO group at the end of polyurethane chains, which results in covalent attachment of ionized PU chains to the surface of MXene via "urethane-like" bonds [21,22]. Finally, add deionized water for emulsification to form hybrid emulsions with PU latex and MXene surface grafted with hydrophilic PU chains. Fig. 1 illustrates the solar-driven film formation process of I-SHWPU. Firstly, the particles are randomly suspended in water. With the evaporation of water, the particles are close to each other and form a tight accumulation. Afterward, the surface protection layer of particles is destroyed, and the particles change from a spherical shape to a rhombic dodecahedron driven by capillary force [23,24]. Under natural visible light, MXene converts solar energy into thermal energy that makes residual moisture evaporate and drives the diffusion of polymer chains cross the boundary of distorted particles. As a result, the interface between particles disappears, and distorted particles completely merge together to form a robust film.

For the preparation of MXene nanosheets. Figs. 2a and 2b show the SEM images of bulky Ti_3AlC_2 before etching and flake-shaped $Ti_3C_2T_x$-MXene exfoliated in the supernatant. The XRD results in Fig. 2e further confirms the successful etching of the Al elements from bulky Ti_3AlC_2, in which the characteristic peaks of Ti_3AlC_2 at $2\theta = 38.8°$ and $2\theta = 9.7°$ disappear, and particularly the peak of Ti_3AlC_2 at $2\theta = 9.7°$ shifts to 6.5° [25]. As shown in Figs. 2c and 2d, the cross-sectional SEM images of SHWPU and I-SHWPU show that the incorporation of MXene roughs the fractured surface but no lumpy aggregates are observed. This implies that our fabrication route yields a well-dispersion of MXene nanosheets in the PU matrix. The XRD curves in Fig. 2e of SHWPU and I-SHWPU further confirm that the MXene nanosheets are uniformly dispersed in the polyurethane matrix. As shown in Fig. 2e, The diffraction peak around 20° is attributed to crystalline PU, which is considered as an ordered structure of the chain segment owing to hydrogen bonds [26]. Moreover, the 6.5° crystal plane diffraction peak of $Ti_3C_2T_x$-MXene does not appear in the I-SHWPU curve. It shows that MXene is uniformly dispersed in the polyurethane matrix.

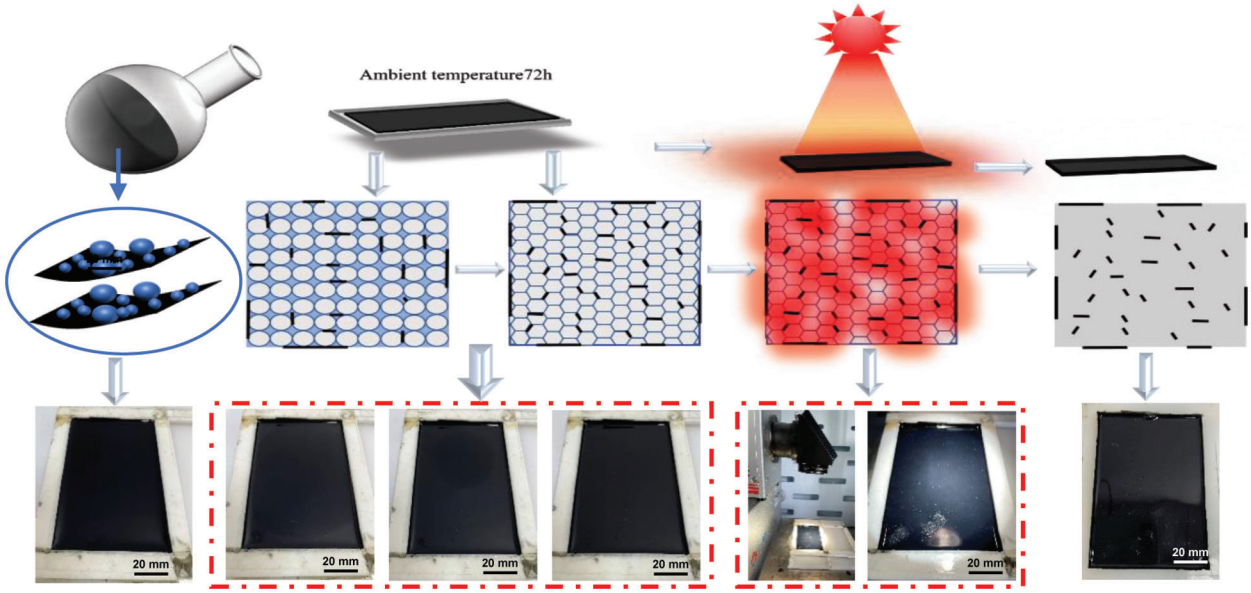

Figure 1: Solar-driven film formation process of I-SHWPU emulsion

Fig. 3a shows the FTIR spectra of MXene, SHWPU, I-SHWPU, and IPDI. It can be seen that MXene consists of -OH groups (3440 cm^{-1}) and Ti-O groups (572 cm^{-1}) [27]. The FTIR spectrum of SHWPU and I-SHWPU shows that the characteristic peak at 2270 cm^{-1} associated with the -NCO group from IPDI is completely disappeared. In addition, the peaks at 3360 cm^{-1} and 1531 cm^{-1} belong to the N-H groups, and the peak around 1720 cm^{-1} is attributed to the vibration of the C=O group [26,28]. In addition, the infrared curves of SHWPU and I-SHWPU are almost identical, indicating that the addition of MXene shows a negligible effect on the molecular structure of the WPU matrix. No characteristic peak of the -OH group is observed, which implies that the diols including the -OH group on the MXene participate in the reaction. This result is consistent with the literature report [20,21]. Raman spectroscopy is used to detect the existence of disulfide in the main chains of WPU [29]. In Fig. 3b, an obvious tensile vibration peak at 510 cm^{-1} associated with disulfide bonds is observed [30]. Fig. 3c shows the particle size distribution of SHWPU, MXene, and I-SHWPU emulsion. The particle size of SHWPU is around 27 nm and the particle size of MXene nanosheets is around 1500 nm. With the combination of MXene and pure WPUs, there are two peaks in the particle size distribution of I-SHWPU. The first peak corresponds with SHWPU, and the second peak complies with MXene. The zeta potential of SHWPU emulsion and MXene aqueous dispersion is about −63 mV and −39 mV, respectively, as shown in Fig. 3d. The high absolute value of zeta potential indicates that there is abundant electrostatic repulsion on the surface of water particles [31]. The zeta potential of the hybrid emulsion reaches −58 mV, indicating well dispersion of MXene against sedimentation in the hybrid emulsion as a result of the surface graft with hydrophilic PU chains to make the surface of MXene with abundant electrostatic repulsion.

In order to confirm the successful grafting of the polyurethane molecular chain to the $Ti_3C_2T_x$-MXene surface, XPS characterization was performed on MXene ($Ti_3C_2T_x$) and modified MXene (I-$Ti_3C_2T_x$). Fig. 4a shows the new peak of N1s associated with the urea bond. The characteristic peak of 400.3 eV appeared in the N1s spectrum of I-$Ti_3C_2T_x$, corresponding to the -NHCOO- bonds. It is indicated that the -NCO at the end of the molecular chain reacts with -OH on the surface of $Ti_3C_2T_x$-MXene. The characteristic peaks of C=O (532.0 eV) and C-O (533, 6 eV) [32,33] in the urethane bond were observed in the O1s spectrum of I-$Ti_3C_2T_x$, which again proved the occurrence of the reaction.

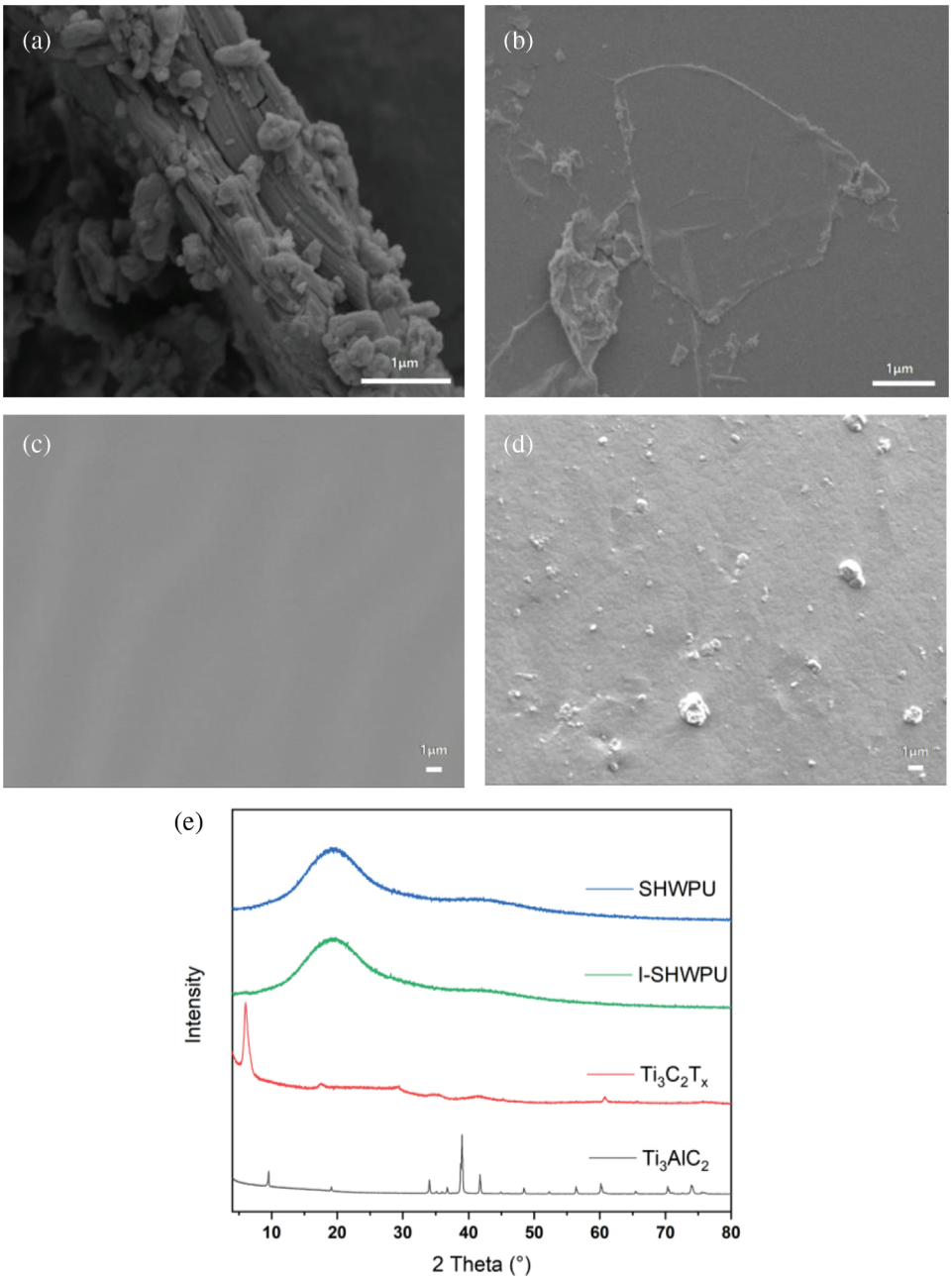

Figure 2: (a, b) SEM image of Ti_3AlC_2 and $Ti_3C_2T_x$-MXene; (c, d) Cross sectional SEM image of SHWPU and I-SHWPU film; (e) XRD curves of SHWPU, I-SHWPU, Ti_3AlC_2 and delaminated $Ti_3C_2T_x$-MXene

Oxidation of MXene is a more serious problem when staying in WPUs as it has been reported that the positively charged edge of MXene would react with water and make MXene turn into titania oxide in humid environment [34]. Fig. 5a shows the study on the oxidative degradation of MXene in the hybrid emulsion. For the purpose of comparison, MXene is also directly mixed into the PU emulsion without any modification. This kind of hybrid emulsion is designated as blended emulsion (B-SHWPU). Fig. 5a demonstrates the observation of two emulsions placed in a UV aging chamber. With increaseing UV exposure time up to 14 days, the color of B-SHWPU emulsion changes from black to transparent dark green, and the color of

MXene sediment at the bottom of the glass bottle is dark brown. This phenomenon indicates that MXene is oxidized in water emulsion. No obvious change in color is observed in I-SHWPU emulsion. With surface graft of ionic polyurethane, MXene is stabilized in water against sediment, and more importantly, is able to resist the corrosion from water. Fig. 5b, the I-SHWPU-1 film is transparent than B-SHWPU-1, and this confirmed the better dispersion of MXene in I-SHWPU. After 14 days, the color of B-SHWPU-14 film becomes transparency. This phenomenon shows that MXene is oxidized in the B-SHWPU emulsion. As shown the Fig. 5c, the absorption of B-SHWPU-14 in the visible light region (410–780 nm) is close to that of SHWPU, which shows that MXene is degraded and oxidized into titanium dioxide. However, the absorption of B-SHWPU-14 in the Ultraviolet region (200–410 nm) is stronger than that of SHWPU owing to the presence of titanium dioxide in B-SHWPU-14 [35]. For I-SHWPU-1 and I-SHWPU-14 films, no obvious difference in color and transparency is observed within the time of 14 days, and the UV-vis absorption almost looks similar.

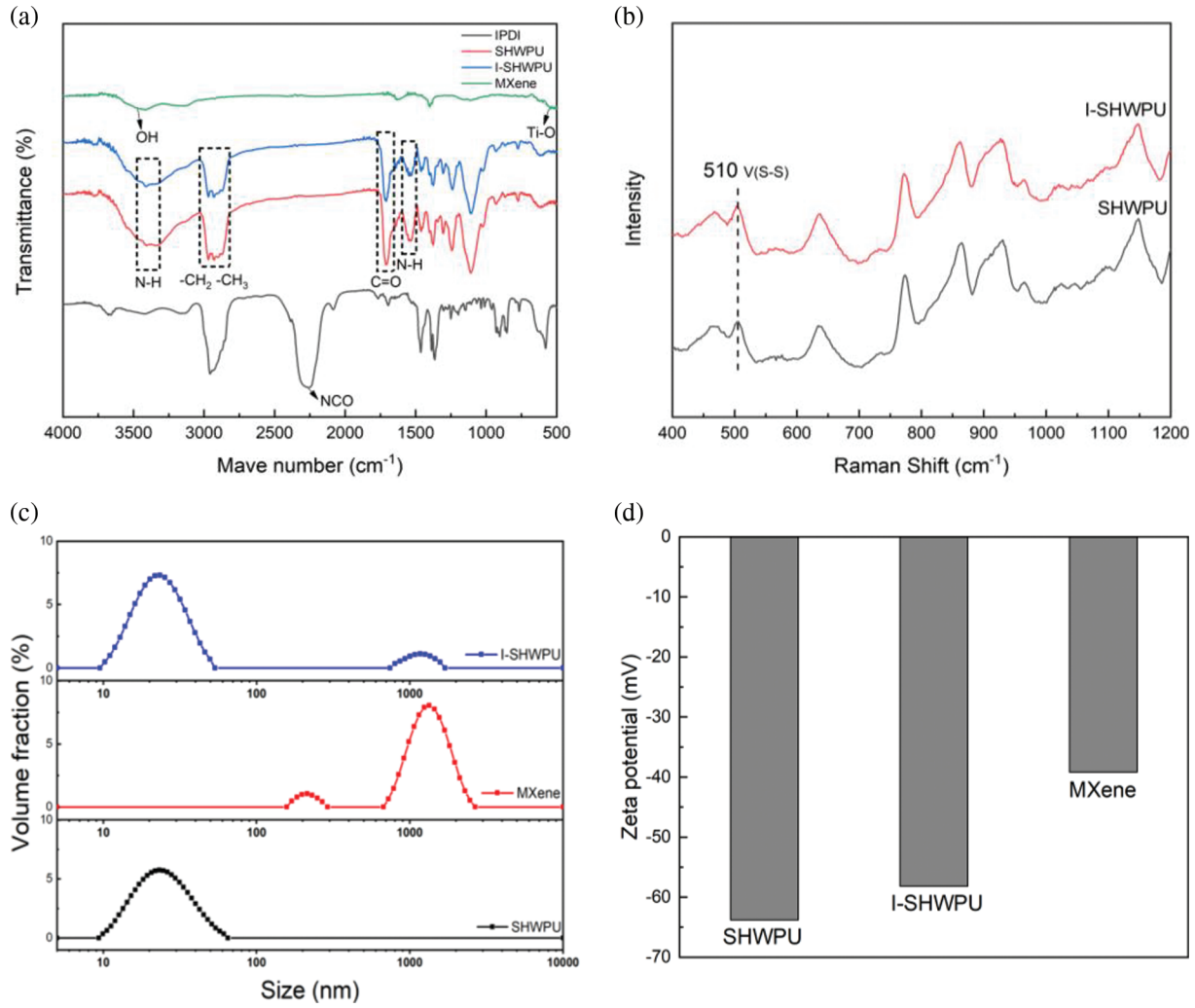

Figure 3: (a) FTIR curves of IPDI, SHWPU, I-SHWPU and MXene; (b) Raman spectrum of SHWPU and I-SHWPU; (c) The particle size distribution curves of SHWPU, MXene and I-SHWPU; (d) Zeta potential of SHWPU, I-SHWPU and MXene

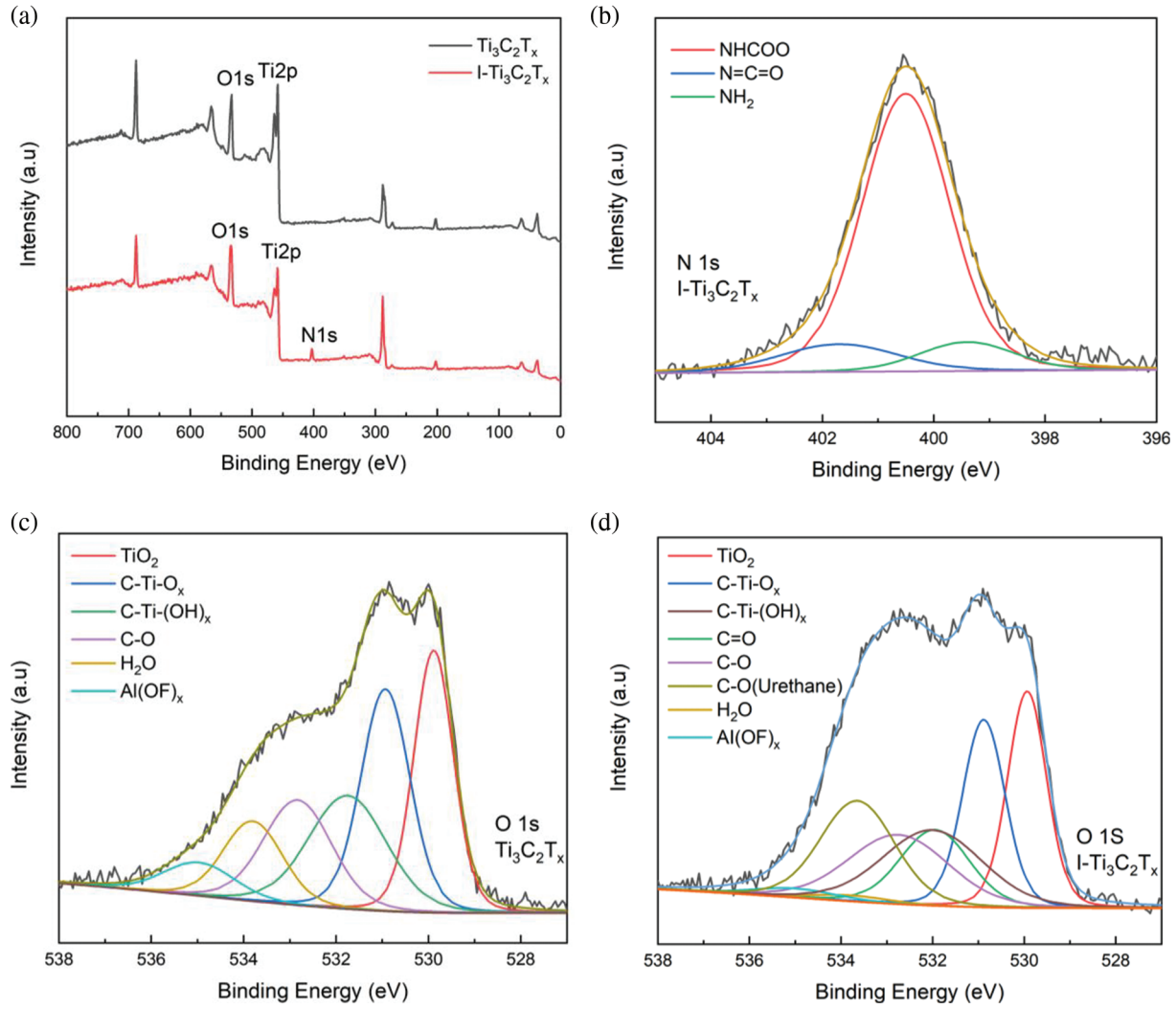

Figure 4: (a) XPS survey spectra of MXene ($Ti_3C_2T_x$) and modified MXene ($I\text{-}Ti_3C_2T_x$); (b, d) show N1s, O1s and spectra for $I\text{-}Ti_3C_2T_x$; (c) shows O1s spectra for $Ti_3C_2T_x$

Thermal infrared images are recorded for revealing the surface temperature evolution of the film exposed to 100 mW/cm^2 visible light irradiation. As shown in Figs. 6a and 6b, the photothermal effect of pure SHWPU film is negligible, whose temperature only reaches 34.3°C after 600 s irradiation with a temperature rise of 10°C. In contrast, the surface temperature of I-SHWPU films rapidly increases from 23.6°C to 40.8°C after 60 s irradiation. The surface temperature can reach 55.3°C after 600 s irradiation. Well-dispersed MXene nanosheets are beneficial for the uniform transfer of heat energy converted from visible light across the films [36]. The covalent chemical bond between MXene and the polyurethane matrix, on the one hand, can improve the interface compatibility between the filler and the matrix, and on the other hand, it can effectively reduce the scattering of interface phonons [37–39]. It is worth noting that MXene in I-SHWPU film still maintains high light-to-heat conversion ability after 6 months, which further supports the long-term stability of MXene in the I-SHWPU film. The mechanical performance of I-SHWPU films is measured to evaluate the effectiveness of solar-driven film formation. Figs. 6c and 6d show that the tensile strength and elongation at break of the reach 3.0 MPa and 650%, respectively. This is competitive with the films formed in an oven at 55°C. Owing to strong interfacial bonding, both tensile strength and yield strength of the film

are improved by over 50% in addition of 0.15% MXene. Therefore, the approach we proposed offers a green solution to the high energy cost of turning polymer emulsions into robust films.

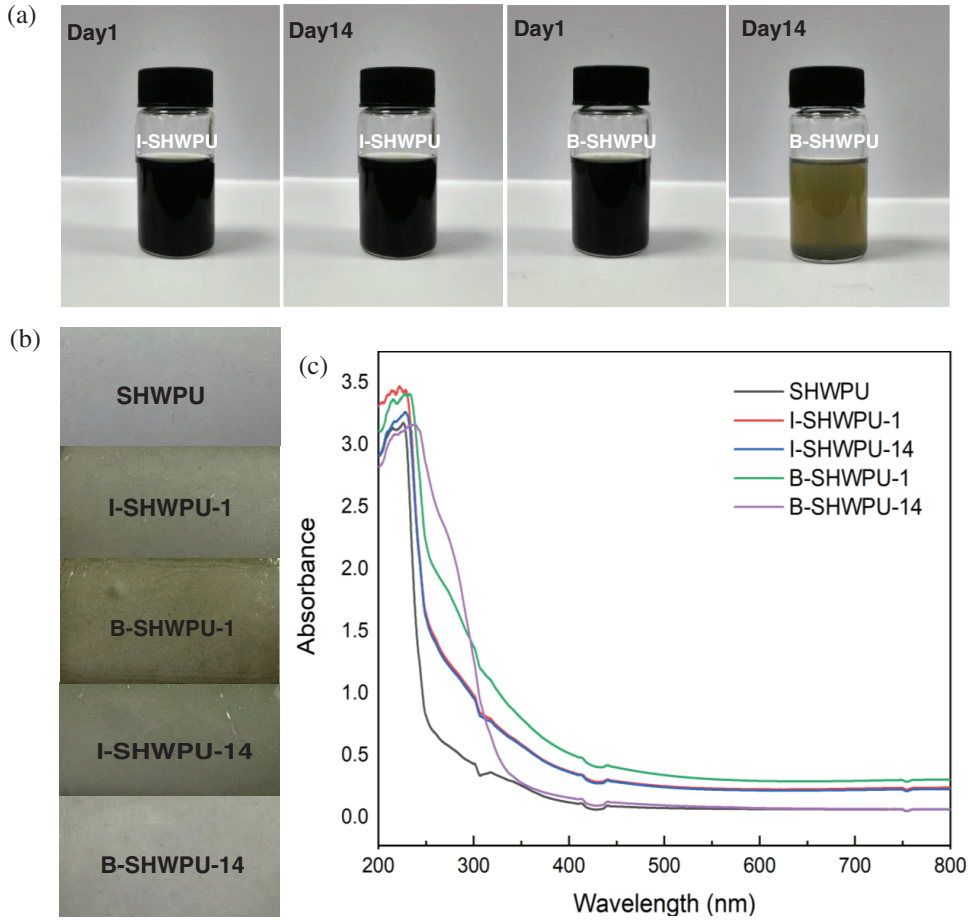

Figure 5: (a) Study on the oxidative degradation of MXene in I-SHWPU and B-SHWPU emulsions under ultraviolet light irradiation; (b) Shows the photos of the dry films (240 ± 10 μm) based on SHWPU, I-SHWPU and B-SHWPU emulsions; (c) The UV-vis absorption spectra of the dry films

DSC experiments were performed to obtain the T_g of SHWPU and I-SHWPU films and to verify the effect of MXene on the molecular chain movement of polyurethane. Fig. 7 shows the DSC curves of SHWPU and I-SHWPU, in which the T_g of the SHWPU and I-SHWPU is around 1°C and 6°C, respectively. The slight increase in T_g indicates that the addition of MXene restricts the movement of molecular chains, which is due to the strong interaction formed between polymer chains and MXene fillers [40].

Studies have shown that the self-healing temperature of disulfide bonds is moderate (50°C–60°C). We have been informed that the temperature of films could rise up to over 50°C when exposed to 100 mW/cm^2 of visible light for 5 min. This offers a suitable condition (50°C–60°C) for the dynamic exchange reaction of disulfide bonding [41]. Therefore, disulfide bonds are introduced into PU chains to offer the films a fast self-healing ability under visible light. A scalpel is used to make a 300 μm-deep scratch on the surface of the. I-SHWPU film. Fig. 8a shows the observation of healing process under optical microscopy. Healing starts at 5 min, and is rapidly completed within 40 min. For molecular-level, the self-healing could be divided into three main stages shown in Fig. 8b. The first stage is dominated by the hydrogen bonds on both

sides of the cracks. Then, the dynamic exchange reaction of disulfide bonds initiated by heat energy converted from solar energy promotes the diffusion between molecular chains, and this results in the mutual cross-linking of fractured surfaces [42,43]. Finally, the healing is completely done by the randomization of molecular chains.

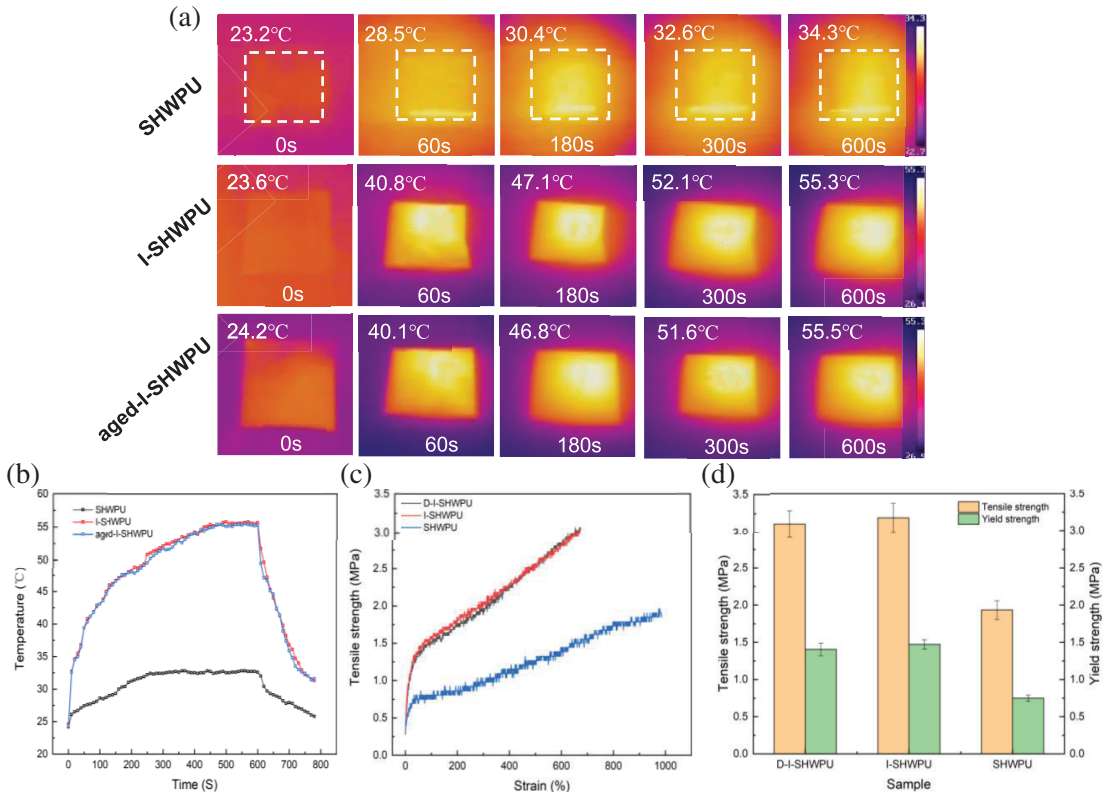

Figure 6: (a) IR thermal images and (b) corresponding surface temperature evolution of SHWPU, I-SHWPU, and aged-I-SHWPU (after 6 months) films under 100 mW/cm^2 visible light; (c) Strain-stress curves of SHWPU, D-I-SHWPU and I-SHWPU; (d) Tensile strength and Yield strength of SHWPU, D-I-SHWPU and I-SHWPU

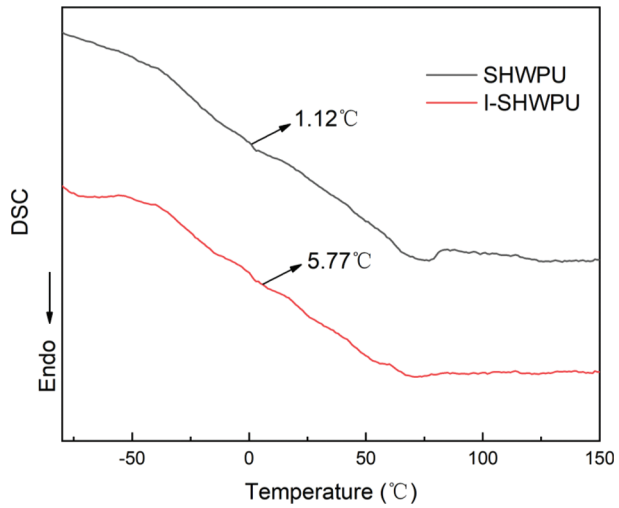

Figure 7: DSC curves of SHWPU and I-SHWPU film

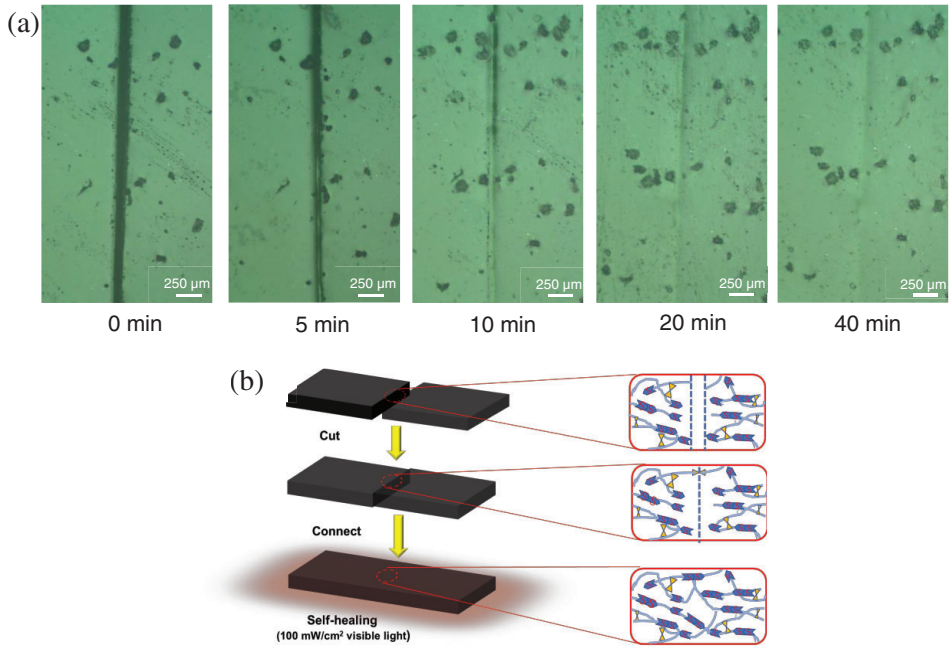

Figure 8: (a) Optical microscopic images of healing process for a scratch in I-SHWPU film at 100 mW/cm^2 visible light; (b) Schematic illustration of self-healing mechanism of I-SHWPU film

In order to study the mechanical properties of the I-SHWPU composite film after healing, we carried out the following self-healing experiments: First, the dumbbell-shaped sample was cut into two sections from the middle, and the cut samples were re-spliced together. Then, the spliced samples were repaired at different times with 100 mW/cm^2 of visible light. Finally, the repaired samples were subjected to tensile experiments to evaluate the repairable performance of the I-SHWPU samples, and the self-healing efficiency can be calculated by using Eq (1).

$$SH\% = \frac{\sigma_{self-healing}}{\sigma_{original}} * 100\% \tag{1}$$

As shown in Figs. 9a and 9b, the self-healing efficiency of the I-SHWPU fractured specimen only reaches 67.20% after 1 h of illumination. With the increase of illumination time, the dynamic exchange of disulfide bonds can be promoted. This can improve the self-healing efficiency of the fracture surface. Finally, through the randomization of PU molecular chains and the dynamic exchange of disulfide bonds, the self-healing of the fracture surface was completed [43]. The tensile strength and elongation at break of the I-SHWPU fractured sample can basically recover to the original level after 2 h of illumination, and the self-healing efficiency can reach more than 94.00%.

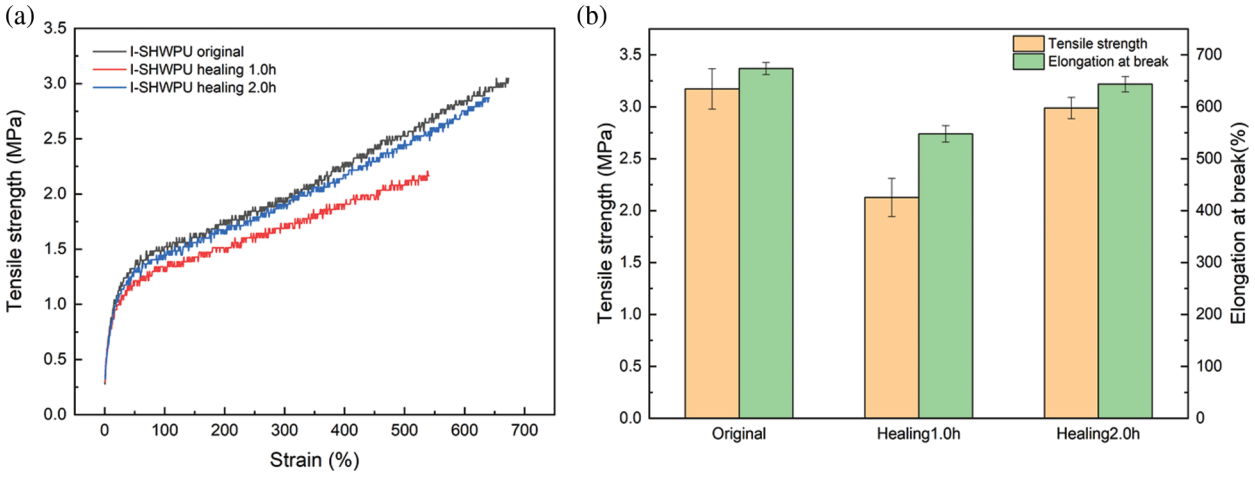

Figure 9: (a) Stress-strain curve of I-SHWPU fracture specimen after healing under 100 mW/cm^2 visible light; (b) Tensile strength and elongation at break of I-SHWPU specimens after healing

4 Conclusions

WPUs are an important class of waterborne polymers in the coating industry. This work reports a facile and scalable route for making stable MXene/PU hybrid emulsions. This just needs to incorporate MXene into the isocyanate-terminated prepolymer before emulsification. This simple operation enables the chemical graft of MXene with carboxylated PU chains and this leads to the stabilization of MXene in PU emulsions both against precipitation and degradation. This is hugely important for applying MXene into the waterborne polymers. Moreover, the covalent connection between MXene and polyurethane improves interface compatibility and effectively reduces interface phonon scattering, and this maximizes the photothermal conversion ability of MXene which makes the formation of robust films possible driven by solar energy. With the introduction of disulfide bonds, the resulting films also could be quickly healed with the input of solar energy. We believe this work would provide a green solution for using WPUs outdoors which is regarded as one of the key hurdles towards the solvent-free coating industry.

Funding Statement: We thank National Natural Science Foundation of China (Grant No. 21503110) for supporting this work.

Conflicts of Interest: The authors declare that they have no conflicts of interest to report regarding the present study.

References

1. Zou, W. J., Liu, J., Bao, X. H., Xiu, G. L. (2019). Comparison of emission standards of volatile organic compounds for coating industry in domestic and foreign areas. *Research of Environmental Sciences, 32(3),* 380–389.
2. Stockwell, C. E., Coggon, M. M., Gkatzelis, G. I., Ortega, J., McDonald, B. C. et al. (2021). Volatile organic compound emissions from solvent-and water-borne coatings-compositional differences and tracer compound identifications. *Atmospheric Chemistry and Physics, 21(8),* 6005–6022. DOI 10.5194/acp-21-6005-2021.
3. Khare, P., Gentner, D. R. (2018). Considering the future of anthropogenic gas-phase organic compound emissions and the increasing influence of non-combustion sources on urban air quality. *Atmospheric Chemistry and Physics, 18(8),* 5391–5413. DOI 10.5194/acp-18-5391-2018.
4. Zhao, Y. C., Chen, M. Z., Wu, S. P., Jiang, Q., Xu, H. Q. et al. (2022). Effects of waterborne polyurethane on storage stability, rheological properties, and VOCs emission of crumb rubber modified asphalt. *Journal of Cleaner Production, 340,* 130682. DOI 10.1016/j.jclepro.2022.130682.

5. Lei, W. Q., Zhou, X., Fang, Q. C., Song, Y. H., Li, Y. G. (2019). Eco-friendly waterborne polyurethane reinforced with cellulose nanocrystal from office waste paper by two different methods. *Carbohydrate Polymers, 209,* 299–309. DOI 10.1016/j.carbpol.2019.01.013.
6. Li, X. G., Xie, Y. B., Huang, M. R., Umeyame, T., Imabhori, H. (2021). Development of clean performance-tunable waterborne polyurethane using acetyl tributyl citrate for transferable holographic films. *Journal of Cleaner Production, 279,* 123496. DOI 10.1016/j.jclepro.2020.123496.
7. David, D. S., Madeleine, W., Willem, U., Myriam, V. (2021). Bio-based waterborne PU for durable textile coatings. *Polymers, 13(23),* 4229. DOI 10.3390/polym13234229.
8. Madbouly, S. (2021). Waterborne polyurethane dispersions and thin films: Biodegradation and antimicrobial behaviors. *Molecules, 26(4),* 961. DOI 10.3390/molecules26040961.
9. Overbeek, A. (2010). Polymer heterogeneity in waterborne coatings. *Journal of Coatings Technology and Research, 7(1),* 1–21. DOI 10.1007/s11998-009-9201-5.
10. Wang, R. T., Li, C. X., Liu, Z. G., Yao, Z. P., Wang, Z. J. et al. (2020). Study of the effect of PGDA solvent on film formation and curing process of two-component waterborne polyurethane coatings by FTIR tracking. *Coatings, 10(5),* 461. DOI 10.3390/coatings10050461.
11. Liu, Y. J. (2002). *The application and study of polyurethane resin*. China. Chemical Industry Press.
12. Hengameh, H. (2018). Waterborne polyurethanes: A review. *Journal of Dispersion Science and Technology, 39(4),* 507–516. DOI 10.1080/01932691.2017.1327818.
13. Morton, O. (2006). Solar energy: A new day dawning?: Silicon valley sunrise. *Nature, 443(7107),* 19–22. DOI 10.1038/443019a.
14. Naguib, M., Kurtoglu, M., Presser, V., Lu, J., Niu, J. J. et al. (2011). Two-dimensional nanocrystals produced by exfoliation of Ti_3AlC_2. *Advanced Materials, 23(37),* 4248–4253. DOI 10.1002/adma.201102306.
15. Halim, J., Kota, S., Lukatskaya, M., Naguib, M., Zhao, M. Q. et al. (2016). Synthesis and characterization of 2D molybdenum carbide (MXene). *Advanced Functional Materials, 26(18),* 3118–3127. DOI 10.1002/adfm.201505328.
16. Zhan, X. X., Si, C., Zhou, J., Sun, Z. M. (2020). MXene and MXene-based composites: Synthesis, properties and environment-related applications. *Nanoscale Horizons, 5(2),* 235–258. DOI 10.1039/C9NH00571D.
17. Xu, D. X., Li, Z. D., Li, L. S., Wang, J. (2020). Insights into the photothermal conversion of 2D MXene nanomaterials: Synthesis, mechanism, and applications. *Advanced Functional Materials, 30(47),* 1–21. DOI 10.1002/adfm.202070314.
18. Lee, Y., Kim, S. J., Kim, Y. J., Lim, Y., Chae, Y. et al. (2020). Oxidation-resistant titanium carbide MXene films. *Journal of Materials Chemistry A, 8(2),* 573–581. DOI 10.1039/C9TA07036B.
19. Huang, S. H., Mochalin, V. N. (2019). Hydrolysis of 2D transition-metal carbides (MXenes) in colloidal solutions. *Inorganic Chemistry, 58(3),* 1958–1966. DOI 10.1021/acs.inorgchem.8b02890.
20. Ding, Y., Xiang, S. L., Zhi, W. Q., Gong, S., He, G. L. et al. (2021). Realizing ultra-stable Ti_3C_2-MXene in aqueous solution via surface grafting with ionomers. *Soft Matter, 17(18),* 4703–4706. DOI 10.1039/D1SM00508A.
21. McDaniel, R. M., Carey, M. S., Wilson, O. R., Barsoum, M. W., Magenau, A. J. D. (2021). Well-dispersed nanocomposites using covalently modified, multilayer, 2D titanium carbide (MXene) and *in-situ* "Click" polymerization. *Chemistry of Materials, 33(5),* 1648–1656. DOI 10.1021/acs.chemmater.0c03972.
22. Wang, Y., Qi, Q. B., Yin, G., Wang, W., Yu, D. (2021). Flexible, ultralight, and mechanically robust waterborne polyurethane/$Ti_3C_2T_x$ MXene/Nickel ferrite hybrid aerogels for high-performance electromagnetic interference shielding. *ACS Applied Materials & Interfaces, 13(18),* 21831–21843 DOI 10.1021/acsami.1c04962.
23. Kobayashi, M., Rharbi, Y., Winnik, M. A. (2001). Effect of inorganic pigments on polymer interdiffusion in a low-T-g latex film. *Macromolecules, 34(6),* 1855–1863. DOI 10.1021/ma000604n.
24. Kim, H. B., Wang, Y. C., Winnik, M. A. (1994). Synthesis, structure and film-forming properties of poly (butyl methacrylate)-poly (methacrylic acid) core-shell latex. *Polymer, 35(8),* 1779–1786. DOI 10.1016/0032-3861 (94)90856-7.
25. Li, L., Zhang, M. Y., Zhang, X. T., Zhang, Z. G. (2017). New Ti_3C_2 aerogel as promising negative electrode materials for asymmetric supercapacitors. *Journal of Power Sources, 364,* 234–241. DOI 10.1016/j.jpowsour.2017.08.029.

26. Lai, X. J., Li, X. R., Wang, L., Shen, Y. D. (2010). Synthesis and characterizations of waterborne polyurethane modified with 3-aminopropyltriethoxysilane. *Polymer Bulletin, 65(1),* 45–57. DOI 10.1007/s00289-009-0233-x.
27. Bezrodna, T., Puchkovska, G., Shymanovska, V., Baran, J., Ratajczak, H. (2004). IR-analysis of H-bonded H_2O on the pure TiO_2 surface. *Journal of Molecular Structure, 700(1–3),* 175–181. DOI 10.1016/j.molstruc.2003.12.057.
28. Zhuo, Y. G., Liu, J., Li, Q. S., Qiu, B., Xing, G. Z. (2016). Preparation and characterization of WPU/CNT/GO nanocomposites. *Integrated Ferroelectrics, 171(1),* 52–58. DOI 10.1080/10584587.2016.1171662.
29. Wan, T., Chen, D. J. (2017). Synthesis and properties of self-healing waterborne polyurethanes containing disulfide bonds in the main chain. *Journal of Materials Science, 52(1),* 197–207. DOI 10.1007/s10853-016-0321-x.
30. Zhang, M. Y., Zhao, F. Q., Xin, W., Luo, Y. J. (2020). Room-temperature self-healing and reprocess able waterborne polyurethane with dynamically exchangeable disulfide bonds. *Chemistries, 5(15),* 4608–4618.
31. Ye, G. B., Jiang, T. (2021). Preparation and properties of self-healing waterborne polyurethane based on dynamic disulfide bond. *Polymers, 13(17),* 2936. DOI 10.3390/polym13172936.
32. Gogolewski, S., Gorna, K. (2008). Structure-property relations and cytotoxicity of isosorbide-based biodegradable polyurethane scaffolds for tissue repair and regeneration. *Journal of Biomedical Materials Research Part A, 85(2),* 456–465. DOI 10.1002/(ISSN)1552-4965.
33. Zhou, S., Hao, G. Z., Zhou, X., Jiang, W., Wang, T. H. et al. (2016). One-pot synthesis of robust superhydrophobic, functionalized graphene/polyurethane sponge for effective continuous oil-water separation. *Chemical Engineering Journal, 302,* 155–162. DOI 10.1016/j.cej.2016.05.051.
34. Natu, V., Hart, J. L. (2019). Edge capping of 2D-MXene sheets with polyanionic salts to mitigate oxidation in aqueous colloidal suspensions. *Angewandte Chemie-International Edition, 58(36),* 12655–12660. DOI 10.1002/anie.201906138.
35. Xiang, B., Jiang, G., Zhang, J. (2015). Surface modification of TiO_2 nanoparticles with silane coupling agent for nanocomposite with poly (butyl acrylate). *Plastics Rubber and Composites, 44(4),* 148–154. DOI 10.1179/1743289815Y.0000000007.
36. Yang, D. Z., Zhou, B., Han, G. J., Feng, Y. Z., Ma, J. M. et al. (2021). Flexible transparent polypyrrole-decorated MXene-based film with excellent photothermal energy conversion performance. *ACS Applied Materials & Interfaces, 13(7),* 8909–8918. DOI 10.1021/acsami.0c20202.
37. Balandin, A. A., Ghosh, S., Bao, W. Z., Calizo, I., Teweldebrhan, D. et al. (2008). Superior thermal conductivity of single-layer grapheme. *Nano Letters, 8(3),* 902–907. DOI 10.1021/nl0731872.
38. Miao, J., Li, H. L., Qiu, H. X., Wu, X., Yang, J. H. (2018). Graphene/PANI hybrid film with enhanced thermal conductivity by in situ polymerization. *Journal of Materials Science, 53(12),* 8855–8865. DOI 10.1007/s10853-018-2112-z.
39. Ding, P., Su, S. S., Song, N., Tang, S. F., Liu, Y. M. et al. (2014). Highly thermal conductive composites with polyamide-6 covalently-grafted graphene by an *in-situ* polymerization and thermal reduction process. *Carbon, 66,* 576–584. DOI 10.1016/j.carbon.2013.09.041.
40. Ariffin, M. M., Aung, M. M., Abdullah, L. C., Salleh, M. Z. (2020). Assessment of corrosion protection and performance of bio-based polyurethane acrylate incorporated with nano zinc oxide coating. *Polymer Testing, 87,* 106526. DOI 10.1016/j.polymertesting.2020.106526.
41. Zhang, M. Y., Zhao, F. Q., Luo, Y. J. (2019). Self-healing mechanism of microcracks on waterborne polyurethane with tunable disulfide bond contents. *ACS Omega, 14(1),* 1703–1714. DOI 10.1021/acsomega.8b02923.
42. Kim, Y. H., Wool, R. P. (1983). A theory of healing at a polymer-polymer interface. *Macromolecules, 16(7),* 1115–1120. DOI 10.1021/ma00241a013.
43. Grande, A. M., Bijleveld, J. C., Garcia, S. J., van der Zwaag, S. (2016). A combined fracture mechanical-rheological study to separate the contributions of hydrogen bonds and disulphide linkages to the healing of poly (urea-urethane) networks. *Polymer, 96,* 26–34. DOI 10.1016/j.polymer.2016.05.004.